

# DOES NONAXISYMMETRIC DYNAMO OPERATE IN THE SUN?

V.V. PIPIN<sup>1</sup> AND A.G. KOSOVICHEV<sup>2,3</sup>

<sup>1</sup>*Institute of Solar-Terrestrial Physics, Irkutsk, 664033, Russian Federation*

<sup>2</sup>*Center for Computational Heliophysics, New Jersey Institute of Technology, Newark, NJ 07102, USA*

<sup>3</sup>*Department of Physics, New Jersey Institute of Technology, Newark, NJ 07102, USA*

## Abstract

We explore effects of random non-axisymmetric perturbations of kinetic helicity (the  $\alpha$  effect) and diffusive decay of bipolar magnetic regions on generation and evolution of large-scale non-axisymmetric magnetic fields on the Sun. Using a reduced 2D nonlinear mean-field dynamo model and assuming that bipolar regions emerge due to magnetic buoyancy in situ of the large-scale dynamo action, we show that fluctuations of the  $\alpha$  effect can maintain the non-axisymmetric magnetic fields through a solar-type  $\alpha^2\Omega$  dynamo process. It is found that diffusive decay of bipolar active regions is likely to be the primary source of non-axisymmetric magnetic fields observed on the Sun. Our results show that non-axisymmetric dynamo models with stochastic perturbations of the  $\alpha$  effect can explain periods of extremely high activity (‘super-cycle’ events) as well as periods of deep decline of magnetic activity. We compare the models with synoptic observations of solar magnetic fields for the last four activity cycles, and discuss implications of our results for interpretation of observations of stellar magnetic activity.

**Keywords:** dynamo; Sun: activity; Sun: magnetic fields; stars: activity; stars: magnetic field; stars: solar-type

## 1. INTRODUCTION

Since the seminal papers of Choudhuri (1992) and Hoyng (1993), random variations of kinetic helicity in dynamo processes (the so-called  $\alpha$  effect) are often considered as the main source of long-term variations of solar activity cycles (Ossendrijver & Hoyng 1996; Moss et al. 2008; Usoskin et al. 2009; Pipin et al. 2012; Passos et al. 2014). In the standard mean-field framework, turbulent generation of magnetic fields results from reflection-symmetry breaking of helical convection motions (Krause & Rädler 1980). In the mean-field theory, the effect is described by the mean-electromotive force,

$$\mathcal{E} = \langle \mathbf{u} \times \mathbf{b} \rangle = \alpha \circ \langle \mathbf{B} \rangle + \dots,$$

where  $\mathbf{u}$  is the turbulent velocity,  $\mathbf{b}$  is the turbulent magnetic field,  $\langle \mathbf{B} \rangle$  is the large-scale magnetic field, and coefficient  $\alpha = -\frac{1}{3} \langle \mathbf{u} \cdot \nabla \times \mathbf{u} \rangle \tau_{\text{cor}}$  is a pseudo-scalar proportional to the kinetic helicity,  $\mathbf{u} \cdot \nabla \times \mathbf{u}$ , and turbulent correlation times,  $\tau_{\text{cor}}$ . The amount of convective energy, which can be spent on turbulent generation of the large-scale magnetic field by the  $\alpha$  effect, is only few percents of the total convective energy (Parker 1979). Taking this constraint into account, it was shown that magnitude of the  $\alpha$  effect can randomly vary in each hemisphere in the range from 10 to 20 percent (see, Choudhuri 1992; Hoyng 1993; Moss et al. 2008). However, the results of Choudhuri (1992) and Ossendrijver & Hoyng (1996) showed that in order to explain the Grand cycles of solar magnetic activity the random fluctuations should be of the same order as the mean magnitude of the  $\alpha$ -effect. Results of Moss et al. (2008) showed that the time scale of fluctuations should also be taken into account. They found that if the correlation time is comparable to the cycle duration then the fluctuations with amplitude of few dozen percents are sufficient to explain the Grand minima of solar activity.

The current paradigm assumes that sunspots are formed from large-scale axisymmetric toroidal magnetic field emerging from the solar convection zone where the field is regenerated by hydromagnetic dynamo. Results of Krause & Rädler (1980) and Raedler (1986) showed that, because of the differential rotation, the solar dynamo can not maintain a regular non-axisymmetric large-scale magnetic field. Nevertheless, large-scale non-axisymmetric magnetic fields are commonly observed on the Sun, for example, in the form of coronal holes (Glencross 1974), which represent

regions of open magnetic flux (Stix 1977). The surface flux-transport models successfully simulate the process of formation of coronal holes from decaying active regions (Wang & Sheeley 1990; Cameron & Schüssler 2017). These models assume that influence of surface non-axisymmetric magnetic fields on the dynamo action in the deep convection zone is negligible. Moss (1999) and Bigazzi & Ruzmaikin (2004) showed that weak large-scale non-axisymmetric field structures may be consistent with non-linear mean field models of the solar dynamo, in which non-axisymmetric dynamo modes are maintained by either non-linearity of  $\alpha$ -effect quenching, or non-axisymmetric distribution of  $\alpha$ . It was suggested that the excitation of the non-axisymmetric modes can be sensitive to the radial dependence of the rotation law (Moss 1999; Pipin 2017). Pipin & Kosovichev (2015) studied response of a nonlinear non-axisymmetric mean-field solar dynamo model to non-axisymmetric perturbations and showed that the effect can depend on the root depth of the non-axisymmetric magnetic fields. The non-axisymmetric dynamo models may be relevant to the problem of solar active longitudes (Berdyugina et al. 2006). Observational results of Stenflo (2012) showed that the presence of background (basal) magnetic flux observed on the surface of the Sun does not depend on the magnetic cycle. From this consideration it seems that much of the basal flux may well originate from the global dynamo. This flux may persist during the solar minima because diffusion of solar bipolar regions could take long time.

In this paper we explore additional possibility which stems from non-axisymmetric dynamo action. Longitudinal fluctuations of the  $\alpha$  effect are usually ignored in mean-field stellar dynamo models. Using nonlinear mean-field dynamo models we show that such non-axisymmetric random perturbations can maintain large-scale non-axisymmetric magnetic fields in a solar-type  $\alpha^2\Omega$  dynamo. Our goal is to investigate the process of stochastic excitation of large-scale non-axisymmetric magnetic field and estimate how it affects the large-scale basal magnetic flux. To compare this mechanism with diffusive decay of bipolar active regions, we simulate active region emergence using the Parker's magnetic buoyancy effect. To demonstrate the difference between the two competitive mechanisms we employ a reduced 2D non-linear and non-axisymmetric dynamo model which describes the dynamo wave propagation on the spherical surface. The modeling results are compared with synoptic observations of large-scale solar magnetic fields on the Sun.

The paper is organized as follows. Section 2 describes the dynamo model and its parameters. Section 3 presents results of numerical simulations for various model conditions. Section 4 gives an outline of observational data and comparison with the model. The final section summarizes and discusses the main results of our analysis.

## 2. NONAXISYMMETRIC 2D DYNAMO MODEL

### 2.1. Governing Equations

In the framework of mean-field magnetohydrodynamics (Krause & Rädler 1980) the evolution of the large-scale magnetic field,  $\langle \mathbf{B} \rangle$ , in perfectly conductive media is governed by the induction equation,

$$\partial_t \langle \mathbf{B} \rangle = \nabla \times (\mathcal{E} + \langle \mathbf{U} \rangle \times \langle \mathbf{B} \rangle), \quad (1)$$

where,  $\mathcal{E} = \langle \mathbf{u} \times \mathbf{b} \rangle$  is the mean electromotive force with  $\mathbf{u}$  and  $\mathbf{b}$  standing for the turbulent velocity and magnetic field respectively. It is convenient (Jennings et al. 1990) to represent the large-scale magnetic field induction vector in terms of the axisymmetric and non-axisymmetric components as follows:

$$\langle \mathbf{B} \rangle = \bar{\mathbf{B}} + \tilde{\mathbf{B}} \quad (2)$$

$$\bar{\mathbf{B}} = \hat{\phi} B + \nabla \times (A \hat{\phi}) \quad (3)$$

$$\tilde{\mathbf{B}} = \nabla \times (\mathbf{r} T) + \nabla \times \nabla \times (\mathbf{r} S), \quad (4)$$

where  $\bar{\mathbf{B}}$  and  $\tilde{\mathbf{B}}$  are the axisymmetric and non-axisymmetric components;  $A$ ,  $B$ ,  $T$  and  $S$  are scalar functions representing the field components;  $\hat{\phi}$  is the azimuthal unit vector,  $\mathbf{r}$  is the radius vector;  $r$  is the radial distance, and  $\theta$  is the polar angle. Hereafter, the overbar denotes the axisymmetric magnetic field, and tilde denotes non-axisymmetric properties.

To elucidate basic properties of the non-axisymmetric dynamo action, we consider a reduced dynamo model in which the radial dependence of the magnetic field is disregarded. In this case, the induction vector of the large-scale magnetic

field is represented in terms of the scalar functions as follows:

$$\begin{aligned} \langle \mathbf{B} \rangle = & -\frac{\mathbf{r}}{R^2} \frac{\partial \sin \theta A}{\partial \mu} - \frac{\hat{\theta}}{R} A + \hat{\phi} B \\ & - \frac{\mathbf{r}}{R^2} \Delta_\Omega S + \frac{\hat{\theta}}{\sin \theta} \frac{\partial T}{\partial \phi} + \hat{\phi} \sin \theta \frac{\partial T}{\partial \mu}, \end{aligned}$$

where  $R$  represents the radius of the spherical surface inside a star where the hydromagnetic dynamo operates. The model employs the following expression of  $\mathcal{E}$ :

$$\mathcal{E} = \alpha \circ \langle \mathbf{B} \rangle - \eta_T \nabla \times \langle \mathbf{B} \rangle + V_\beta \hat{\mathbf{r}} \times \mathbf{B}. \quad (5)$$

Here, it is assumed that:

$$\alpha_{ij} = \alpha_0 \psi(|\langle \mathbf{B} \rangle|) \cos \theta \delta_{ij}, \quad (6)$$

where coefficient  $\alpha_0$  represents the magnitude of the  $\alpha$ -effect, and  $\psi$  is the standard magnetic quenching function (Pipin 2008). The magnitude,  $\alpha_0$ , is allowed to vary randomly in time  $t$  and longitude  $\phi$ :

$$\alpha_0 = \bar{\alpha} (1 + \xi_\alpha(\phi, t)), \quad (7)$$

where  $\bar{\alpha}$  is the stationary axisymmetric part of  $\alpha$ -effect; the function  $\xi_\alpha(\phi, t)$  describes random fluctuations. Details of the fluctuations will be defined further. The second term represents turbulent diffusion with coefficient  $\eta_T$ . The last term in Eq (5) describes the magnetic buoyancy effect. Here,  $\hat{\mathbf{r}}$  is the radial unit vector, and  $V_\beta$  is the escape velocity of magnetic field, The escape velocity,  $V_\beta$ , accounts for the loss of generated magnetic flux from the dynamo region (Parker 1984; Noyes et al. 1984; Moss et al. 1990). Parker (1979) suggested that the magnetic buoyancy can result in formation of bipolar active regions. Currently, it becomes evident that the magnetic buoyancy is not the only mechanism forming emerging active regions of the Sun (Getling 2001; Kitiashvili et al. 2010; Stein & Nordlund 2012; Leka et al. 2013; Brandenburg et al. 2013; Losada et al. 2017; Martin 2018). In this study, we assume that the magnetic buoyancy acts on relatively small-scale parts of the axisymmetric magnetic field, perhaps, because of some kind of nonlinear instability, and contributes to generation of the non-axisymmetric magnetic field component. It is formulated following Kitchatinov & Pipin (1993):

$$V_\beta = \begin{cases} \frac{\alpha_{MLT} u'}{\gamma} \beta^2 K(\beta) [1 + \xi_\beta(\phi)], & \text{if } \beta \geq \beta_{cr}, \\ 0, & \text{if } \beta < \beta_{cr} \end{cases} \quad (8)$$

where  $\beta = |\langle \mathbf{B} \rangle| / B_{eq}$ ,  $B_{eq} = \sqrt{4\pi \bar{\rho} u'^2}$ , function  $K(\beta)$  is defined in Kitchatinov & Pipin (1993), function  $\xi_\beta(\phi)$  describes the longitudinal dependence of the instability, and parameter  $\beta_{cr}$  controls the instability threshold. These parameters will be described below. From results of the above cited paper, it follows that for  $\beta \ll 1$ ,  $K(\beta) \sim 1$ , and for  $\beta > 1$ ,  $K(\beta) \sim 1/\beta^3$ . In this formulation, the preferable latitude of the “active region emergence” is determined by maximum of the toroidal magnetic field energy, see Eq.(8). Parameter  $\beta_{cr} = 0.5$  is used to prevents emergence of active regions at high latitudes.

The minimal set of the dynamo equations to model the non-axisymmetric magnetic field evolution can be obtained by generalization of the 1D model suggested by Parker (1993), which has a solution in the form of dynamo waves migrating towards the equator. The model studied extensively, for example, by Kuzanyan (1998); Moss et al. (2008); Usoskin et al. (2009). In this framework, the radial dependence of magnetic field is disregarded, and it is assumed that the radial gradient of angular velocity is greater than the latitudinal gradient. Applying these simplifications to Eq (1) and Eqs (2-4) we obtain the following set of dynamo equations in terms of the scalar functions,  $A, B, S$ , and  $T$ :

$$\begin{aligned} \partial_t B = & -\sin \theta \frac{\partial \Omega}{\partial r} \frac{\partial (\sin \theta A)}{\partial \mu} + \eta_T \frac{\sin^2 \theta}{R^2} \frac{\partial^2 (\sin \theta B)}{\partial \mu^2} - \frac{B}{\tau} \\ & + \frac{\sin \theta}{R} \frac{\partial}{\partial \mu} \alpha_0 \mu \langle B_r \rangle + \frac{\alpha_0 \mu}{R} \langle B_\theta \rangle - \frac{1}{R} V_\beta \langle B_\phi \rangle \end{aligned} \quad (9)$$

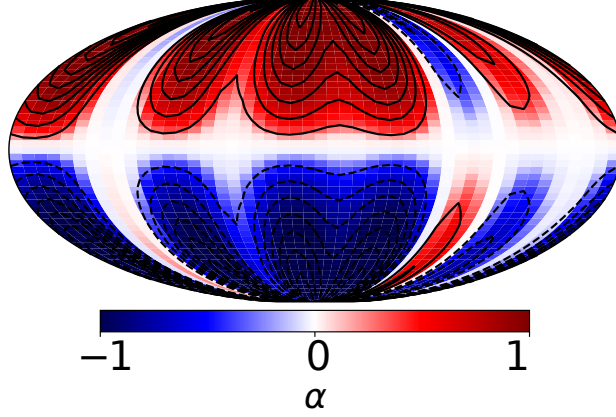


**Figure 1.** Snapshot of a random realization of the  $\alpha$  effect with  $\sigma_\xi = 0.25$  (see, Sec. 2.2). Contours are drawn in range of  $\pm 2$ .

$$\partial_t A = \alpha_0 \mu \langle B_\phi \rangle + \eta_T \frac{\sin^2 \theta}{R^2} \frac{\partial^2 (\sin \theta A)}{\partial \mu^2} - \frac{V_\beta}{R} A - \frac{A}{\tau}, \quad (10)$$

$$\begin{aligned} \partial_t \Delta_\Omega T + \Delta_\Omega \delta \Omega \frac{\partial T}{\partial \phi} = & -\frac{1}{R} \frac{\partial \Omega}{\partial r} \sin^2 \theta \frac{\partial \Delta_\Omega S}{\partial \mu} + \frac{\eta_T}{R^2} \Delta_\Omega^2 T \\ & + \Delta_\Omega \frac{\alpha_0 \mu}{R} (\langle B_r \rangle \sin^2 \theta + \mu \sin \theta \langle B_\theta \rangle) - \frac{1}{R} \frac{\partial}{\partial \phi} \left[ \frac{\alpha_0}{\sin \theta} \mu \langle B_\phi \rangle \right] \\ & + \frac{1}{R} \frac{\partial}{\partial \mu} \alpha_0 \mu \sin \theta \{ \mu \sin \theta \langle B_r \rangle + \mu^2 \langle B_\theta \rangle \} \\ & - \frac{1}{R \sin \theta} \frac{\partial}{\partial \phi} \langle B_\theta \rangle V_\beta - \frac{\partial}{\partial \mu} (\sin \theta \langle B_\phi \rangle V_\beta), \end{aligned} \quad (11)$$

$$\begin{aligned} \partial_t \Delta_\Omega S + \left( \delta \Omega \Delta_\Omega \frac{\partial}{\partial \phi} S \right) = & \frac{\eta_T}{R^2} \Delta_\Omega^2 S + \frac{\partial}{\partial \mu} \alpha_0 \mu \sin \theta \langle B_\phi \rangle \\ & + \frac{\partial}{\partial \phi} \left\{ \frac{\alpha_0 \mu}{\sin \theta} (\langle B_\theta \rangle + \sin \theta (\mathbf{e} \cdot \langle \mathbf{B} \rangle)) \right\} \\ & - \frac{1}{\sin \theta} \frac{\partial}{\partial \phi} (\langle B_\phi \rangle V_\beta) + \frac{\partial}{\partial \mu} (\sin \theta \langle B_\theta \rangle V_\beta), \end{aligned} \quad (12)$$

where  $\Delta_\Omega = \frac{\partial}{\partial \mu} \sin^2 \theta \frac{\partial}{\partial \mu} + \frac{1}{\sin^2 \theta} \frac{\partial^2}{\partial \phi^2}$  and  $\mu = \cos \theta$ . The  $\tau$ -terms in Eqs(9,10) were suggested by Moss et al. (2008)

to account for turbulent diffusion in radial direction. Similarly to the cited paper we put  $\tau = 3 \frac{R^2}{\eta_T}$ . The  $\tau$ -parameter will be specified in the next subsection. For brevity, some terms in above equations are given explicitly via components of the magnetic induction vector,  $\langle \mathbf{B} \rangle$ . These terms result in coupling between different modes of the large-scale magnetic field in the case of longitudinal dependence of parameters  $\alpha_0$  and  $V_\beta$ . If the differential rotation is strong then the non-axisymmetric modes are stable against the dynamo instability. The nonlinear coupling (e.g., due to the  $\alpha$ -effect) is not very effective for maintaining non-axisymmetric dynamo modes (Brandenburg et al. 1989; Raedler et al. 1990; Moss 1999; Pipin & Kosovichev 2015). To simulate stretching of non-axisymmetric magnetic field by the surface differential rotation we consider the latitudinal dependence of angular velocity  $\delta \Omega = -0.25 \sin^2 \theta \Omega$  in Eqs (11) and (12), which are written in the coordinate system rotating with angular velocity  $\Omega$ . In this paper, we discuss relatively simple 2D models with the constant rotational shear.

The numerical scheme employs a pseudo-spectral approach for integration along latitude. For the non-axisymmetric components, we employ the spherical harmonic decomposition, i.e., scalar functions  $T$  and  $S$  are represented in the

form:

$$T(\mu, \phi, t) = \sum \hat{T}_{\ell, m}(t) \bar{P}_{\ell}^{|m|} \exp(-im\phi), \quad (13)$$

$$S(\mu, \phi, t) = \sum \hat{S}_{\ell, m}(t) \bar{P}_{\ell}^{|m|} \exp(-im\phi), \quad (14)$$

where  $\bar{P}_{\ell}^m$  is the normalized associated Legendre function of degree  $\ell \geq 1$  and azimuthal order  $m \geq 1$ . Note that  $\hat{S}_{\ell, -m} = \hat{S}_{\ell, m}^*$ , and the same is valid for  $\hat{T}$ . Our typical simulation runs were performed for 990 spherical harmonics (with  $\ell_{max} = 36$ ,  $m_{max} = 18$ ). In addition, some runs were performed with higher resolution including 1752 spherical harmonics ( $\ell_{max} = 48$ ,  $m_{max} = 24$ ). All the nonlinear terms are calculated explicitly in the real space. The numerical integration is carried out in latitude from pole to pole.

To quantify asymmetry of the mean radial magnetic field distribution relative to the equator, we introduce the parity index,  $P_E$ :

$$P_E = \frac{E_q - E_d}{E_q + E_d}, \quad (15)$$

$$E_d = \frac{1}{4} \int (\bar{B}_r(\mu) - \bar{B}_r(-\mu))^2 d\mu,$$

$$E_q = \frac{1}{4} \int (\bar{B}_r(\mu) + \bar{B}_r(-\mu))^2 d\mu,$$

where  $E_d$  and  $E_q$  are the energy of the antisymmetric and symmetric modes, respectively.

We consider decomposition of the radial magnetic field into dynamo modes:

$$\langle \mathbf{B}_r \rangle = \sum B_r^{(m)}(\mu) e^{im\phi},$$

where the case of  $m = 0$  corresponds to the axisymmetric magnetic field. The degree of non-axisymmetry of the magnetic field is described by the ratio:

$$P_X = \frac{\tilde{E}_r^{(m)}}{E_r^{(m)}}, \quad (16)$$

$$\tilde{E}_r^{(m)} = \frac{1}{8\pi} \sum_{m \geq 1} \int B_r^{(m)} B_r^{(m)*} d\mu, \quad (17)$$

and  $E_r^{(m)}$  is the total energy of the radial component of magnetic field. Other characterization parameters are the mean strength of the unsigned radial magnetic field:  $|\langle \mathbf{B}_r \rangle| = \sqrt{E_r^{(m)}/2\pi}$ , and the unsigned toroidal magnetic field:  $|\langle \mathbf{B}_{\phi} \rangle| = \sqrt{E_{\phi}^{(m)}/2\pi}$ , where  $E_{\phi}^{(m)}$  is the total energy of the toroidal component. The similar parameters are introduced for the axisymmetric magnetic field.

## 2.2. Nonaxisymmetric perturbations

Variations of the  $\alpha$ -effect are modeled by Eq. (7). The time scales in our model is defined in terms the characteristic diffusion time,  $\frac{R^2}{\eta_T}$ . In these units, the basic dynamo period (corresponding to the 11-year cycle) is  $P \approx 0.15 \frac{R^2}{\eta_T}$ . The fluctuations are imposed randomly in time. We consider both, short and long correlation times. For the solar case, the short correlation time,  $\tau_{\xi} = 0.02P$ , is roughly equal to the correlation time of non-axisymmetric modes of solar magnetic fields (Pipin et al. 2014). In addition, we consider the long correlation time,  $\tau_{\xi} = 0.5P$ . The longitudinal dependence of function  $\xi_{\alpha}(\phi, t)$  is modeled as a superposition of sinusoidal oscillations with random amplitudes and phases. The strength of fluctuations is controlled by parameter  $\sigma_{\xi}$  which is the standard deviation (STD) of the random variable,  $\xi_{\alpha}$ . As in the model of Pipin & Sokoloff (2011), we consider a set of  $\sigma_{\xi} = 0.25, 0.5, 1$  for the short and long correlation time  $\tau_{\xi}$  cases. The longitudinal fluctuations of the  $\alpha$  effect are modeled as a superposition of random harmonics up to the octupole modes.

In practice, the fluctuations of the  $\alpha$  effect are implemented as follows. We use the pseudo-random number generator library of SciPy (scipy.org) to produce a Gaussian set of random intervals with correlation time  $\tau_{\xi}$ . Then, during the

**Table 1.** Parameters of the dynamo models,  $P$  is the dynamo period.

Model	$C_\beta$	$\sigma_\xi$	$\tau_\xi/P$
M0	0	0	-
M1a	40	0	-
M1b	0	0.25	0.02
M2a	40	0.25	0.02
M2b	40	0.5	0.02
M2c	40	1.	0.02
M2d	40	1. , $\tilde{\xi}_\alpha = 0$	0.02
M3a	40	0.25	0.5
M3b	40	0.25, $\tilde{\xi}_\alpha = 0$	0.5

dynamo run, the distribution of  $\xi_\alpha(\phi, t)$  is calculated for each of the random time intervals. In this step, we generate a random Gaussian sequence of length  $N_\phi$  (the number of mesh points in azimuth) with the STD of  $N_\phi\sigma_\xi$ . Then, using the fast Fourier transform we filter out all harmonics higher than the octupole. The obtained distribution of  $\xi_\alpha(\phi, t)$  is used in the model until the next random fluctuation. A snapshot of a random realization of  $\alpha$  is illustrated in Figure 1.

Magnetic buoyancy instability perturbations are determined by function:

$$\xi_\beta(\phi) = C_\beta \exp\left(-m_\beta \sin^2\left(\frac{\phi - \phi_0}{2}\right)\right). \quad (18)$$

The instability is randomly initiated in the northern or southern hemispheres, and the longitude,  $\phi_0$ , is also chosen randomly. We arbitrary chose the fluctuation interval  $\tau_\beta = 0.01P$ . After injection of the perturbation the evolution is solely determined by the dynamo equations. Parameter  $m_\beta$  controls the spatial scale of the instability. Theoretically, using a high values of  $m$  we can reproduce the spatial scale of the solar active regions. However, this requires increasing the resolution in both longitude and latitude, and becomes computationally expensive. We chose the value  $m_\beta = 50$ , which allows us to accurately resolve the evolving non-axisymmetric perturbations of magnetic field, and qualitatively reproduce the essential physical effects. Parameter  $C_\beta$  controls the amount of the injected magnetic flux. If large-scale toroidal magnetic flux at a given co-latitude  $\theta$  is transformed into magnetic flux of the perturbation then  $\langle \xi_\beta(\phi, t) \rangle_\phi \approx 1$ . This condition corresponds to  $C_\beta \approx 15$ . In reality, solar active regions are formed by concentration of the toroidal magnetic flux emerging in the photosphere. Turbulent convective motions and other physical processes may take part in the process of formation of solar active regions. Therefore, parameter  $C_\beta$  can be higher than the above mentioned value, and we choose it about three times greater  $C_\beta = 40$  than the value corresponding to the local large-scale field. In the numerical experiments, we found that higher values of  $C_\beta$  result in strong cycle-to-cycle variability of the magnetic energy even in the case of stationary  $\alpha$ -effect. For the chosen  $C_\beta$ ,  $|\langle \mathbf{B} \rangle| \approx 2|\overline{B_\phi}|$ , therefore fluctuations of the magnetic field because of the magnetic buoyancy instability are of the order of the axisymmetric toroidal magnetic field strength, which is widely accepted in the literature (Krause & Rädler 1980; Brandenburg & Subramanian 2005). This part of the model can be improved using the bipolar region production algorithms from the flux-transport models.

Equations (9-12) are solved numerically in the non-dimensional form. As in the model of Moss et al. (2008), we assume that the rotational shear is constant in latitude. The effect of differential rotation is controlled by non-dimensional parameter  $R_\omega = \frac{R^2}{\eta_T} \frac{\partial \Omega}{\partial r}$ , the  $\alpha$ -effect is measured by parameter  $R_\alpha = \frac{R\bar{\alpha}}{\eta_T}$ , the magnetic buoyancy depends on  $R_\beta = \frac{R}{\eta_T} \frac{\alpha_{MLT} u'}{\gamma}$ , and the magnetic field is measured relative to the equipartition strength  $B_{eq} = \sqrt{4\pi \rho u'^2}$ . Following



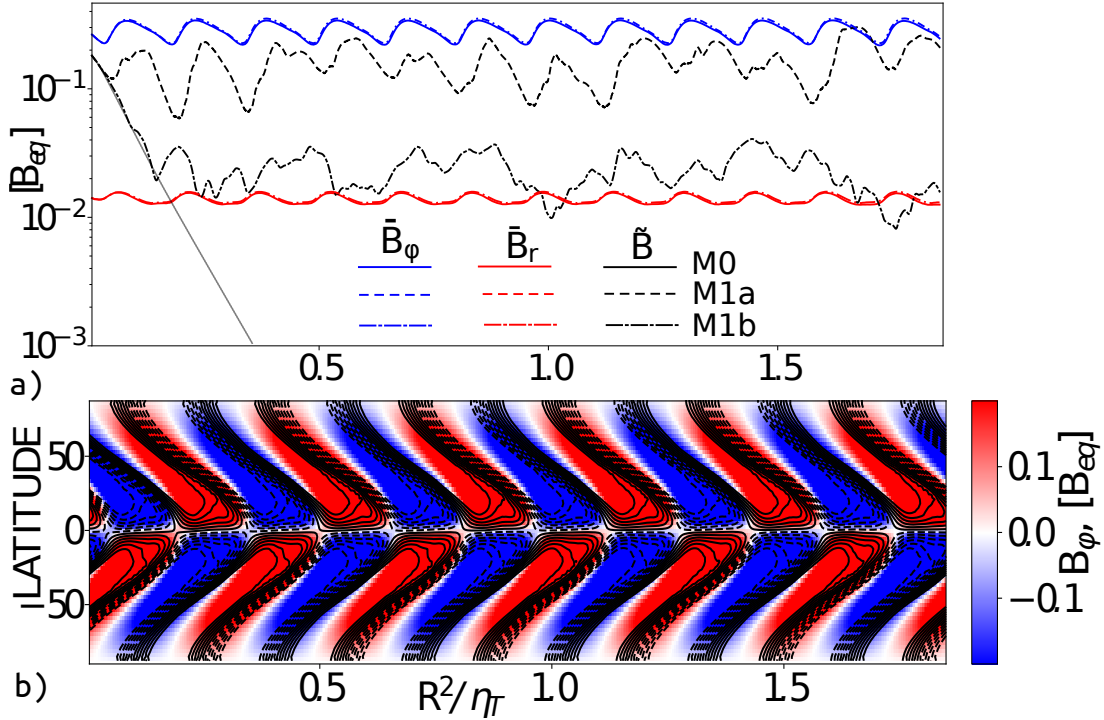


**Figure 2.** a) Comparison of models M0 (solid lines), M1a (dash lines) and M1b (dash-dot lines).  $\bar{B}_\phi$  (blue) and  $\bar{B}_r$  (red) are the mean axisymmetric toroidal and radial magnetic field,  $\bar{B}$  (black) is the mean non-axisymmetric magnetic field in the units of the equipartition field strength. The parameters of the axisymmetric magnetic field in the models are very similar. b) The time-latitude diagram of the toroidal magnetic field (background image) and the radial magnetic field (contours are in the range of  $\pm 0.002$ ) for model M1a.

Pipin & Sokoloff (2011) we put  $R_\omega = \frac{R\Omega}{\eta_T} = 10^3$ ,  $R_\alpha = 1$ . This choice describes the  $\alpha^2\Omega$  dynamo regime with differential rotation as the main driver of axisymmetric toroidal magnetic field. The non-axisymmetric modes do not take part in the dynamo unless some non-axisymmetric phenomena come into the play. To estimate the magnetic buoyancy parameter we employ results of Kitchatinov & Pipin (1993) who argued that the maximum buoyancy velocity of large-scale magnetic field of equipartition strength  $B_{eq}$  is of the order of 6 m/s. In the solar conditions, the magnetic diffusion  $\eta_T = 10^{12} \text{cm}^2/\text{s}$  (Martinez Pillet et al. 1993; Rüdiger et al. 2011), and  $R_\beta \approx 500$ . In our models, the large-scale magnetic field strength is below  $B_{eq}$ . Hence, we use by an order of magnitude smaller value:  $R_\beta = 50$ . In addition to nonlinear quenching of the  $\alpha$ -effect, the magnetic buoyancy also causes a nonlinear saturation of the dynamo process.

Table 1 shows the variable parameters of our models:  $C_\beta$  controls active region emergence by means of the Parker’s magnetic buoyancy instability;  $\sigma_\xi$  is the STD of the random  $\alpha$  effect;  $\tau_\xi$  is the correlation time of the random  $\alpha$  fluctuations, measured relative to dynamo period  $P$ . In models M2d and M3b, non-axisymmetric perturbations of  $\alpha$  are neglected:  $\tilde{\xi}_\alpha = 0$  (however, the axisymmetric  $\alpha$  component fluctuates). For the chosen set of parameters, the antisymmetric parity is dominant in stationary dynamo regimes of models M0 and M1a. The magnetic field distribution of model M1a in the stationary stage is used as the initial condition for subsequent runs.

### 3. NUMERICAL RESULTS

Figure 2 shows evolution of dynamo properties in the reference models, M0 and M1a,b. The mean toroidal magnetic field varies around  $0.4B_{eq}$ , while the radial magnetic field is by a factor of 50 smaller. Model M0 shows that the non-axisymmetric magnetic field is decaying with time. Model M1a maintains large-scale non-axisymmetric magnetic field which is seeded by diffusive dispersion of bipolar active regions. The mean strength of the non-axisymmetric magnetic field is a bit less or around the mean strength of the axisymmetric toroidal magnetic field. Interesting that the non-axisymmetric perturbations almost do not affect the axisymmetric magnetic field evolution. However, randomness of the active region formation results in some randomness of the overall magnetic activity.

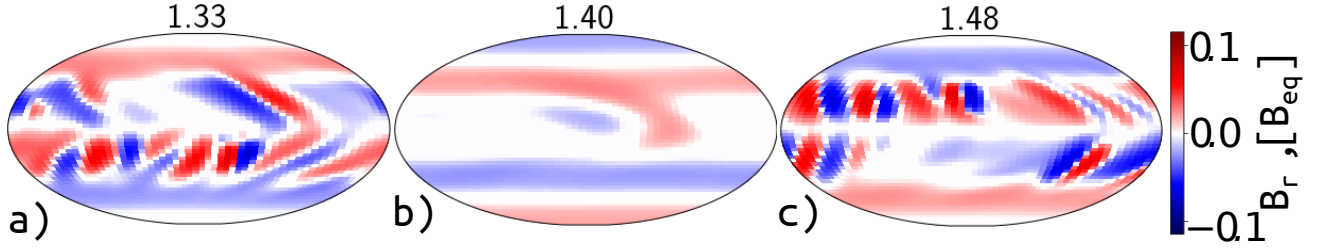


**Figure 3.** Snapshots of the radial magnetic field distribution in model M1a.

Time-latitude diagrams of the axisymmetric toroidal and radial magnetic fields for models M0 and M1a,b are very similar. Figure 2b shows the diagrams for model M1a. We see that the model correctly reproduces the solar-like dynamo waves of toroidal magnetic field which drifts to the equator during the magnetic cycle. However, the time-latitude evolution of radial magnetic field does not show the polar branch (cf., Stenflo & Guedel 1988). Also, the phase relation between the radial and toroidal components does not correspond to observations. The observations, e.g., the above cited paper and Stenflo (2013) or Blackman & Brandenburg (2003), show that  $\overline{B_r} \overline{B_\phi} < 0$  at low latitudes of the Sun.

Figure 3 shows snapshots of the radial magnetic field distribution for different phases of the magnetic cycle in model M1a. These snapshots show some solar-like features in organization of the bipolar regions, such as the hemispheric Hale polarity rule. It is driven by the axisymmetric toroidal magnetic field. Diffusive decay of the bipolar regions and the differential rotation produce large-scale unipolar regions which may extend from one hemisphere to another, as seen in Figure 3a showing a snapshot for the magnetic cycle maximum. Figure 3b shows that some remnants of the bipolar regions can survive during the magnetic cycle minimum.

Model M1b shows (Figure 2a, dash-dot line) that short-term stochastic fluctuations of the  $\alpha$  effect with  $\sigma_\xi = 0.25$  generate an order of magnitude smaller non-axisymmetric magnetic field than the bipolar regions in model M1a. Model M1a shows the magnetic cycle modulation of the mean strength of the non-axisymmetric magnetic field. This feature is seen in the observations (see Sec. 4). But, it is absent in the stochastic non-axisymmetric dynamo models. The non-axisymmetric dynamo is sustained by either non-axisymmetric magnetic buoyancy instability (e.g., model M1a) or the non-axisymmetric perturbations of the  $\alpha$  effect (model M1b). Model M0 shows that the nonaxisymmetric magnetic field vanishes if these two effects are simultaneously neglected. The large-scale non-axisymmetric magnetic field in model M1b is sustained by the non-axisymmetric fluctuations of the  $\alpha$  effect (cf the results of model M0). In this case, the magnetic buoyancy of the axisymmetric magnetic field does not significantly affect the results. Also, the nonlinear interaction between the non-axisymmetric modes due to magnetic buoyancy is small because the strength of the non-axisymmetric components is well below the equipartition value.

Figure 4 shows results for the dynamo models which combine effects of the bipolar regions and stochastic non-axisymmetric dynamo. Models M2a and M2b employ a moderate level of short-term  $\alpha$  fluctuations with  $\sigma_\xi = 0.25$  and  $\sigma_\xi = 0.5$  respectively. In both cases, perturbations of the axisymmetric dynamo mode are not strong. This is compatible with the results of the standard 1D models (e.g., Choudhuri 1992; Hoyng 1993; Moss et al. 2008), which showed that small short-term fluctuations of the  $\alpha$ -effect in  $\alpha\Omega$  dynamo models do not lead to substantial variations of the magnetic cycle. Contrary, Figures 4c and d show that the radial magnetic field experiences strong noisy perturbations. In particular, model M2b shows this in both the equatorial and radial regions. The degree of non-axisymmetry of magnetic activity, parameter  $P_X$ , varies from about zero during the minima to 0.95 during the maxima of magnetic cycles. It is found that with the increase of  $\sigma_\xi$  the amount of non-axisymmetric magnetic field during the cycle minimum increases. Another interesting effect is that the combined action of the bipolar regions and non-axisymmetric perturbations of the  $\alpha$ -effect can result in magnetic parity violations. Model M2b shows stronger deviation of parameter  $P_E$  from  $-1$  than model M2a. The effect becomes clear in model M2c with strong fluctuations of the  $\alpha$ -effect,  $\sigma_\xi = 1$ .

This effect is demonstrated in Figure 5. Model M2c shows strong cyclic variations of the mean total strength of toroidal magnetic field. In some cases the two subsequent cycles are merged in one super cycle. In such cycle, the total magnetic field strength exceeds the strength of the background toroidal magnetic field by a factor of 2. The basal level of non-axisymmetric magnetic field is well above zero especially in the activity minima before and after the super cycle. Perturbations of the magnetic parity in model M2c are much higher than in models M2a and M2b. Model M2d



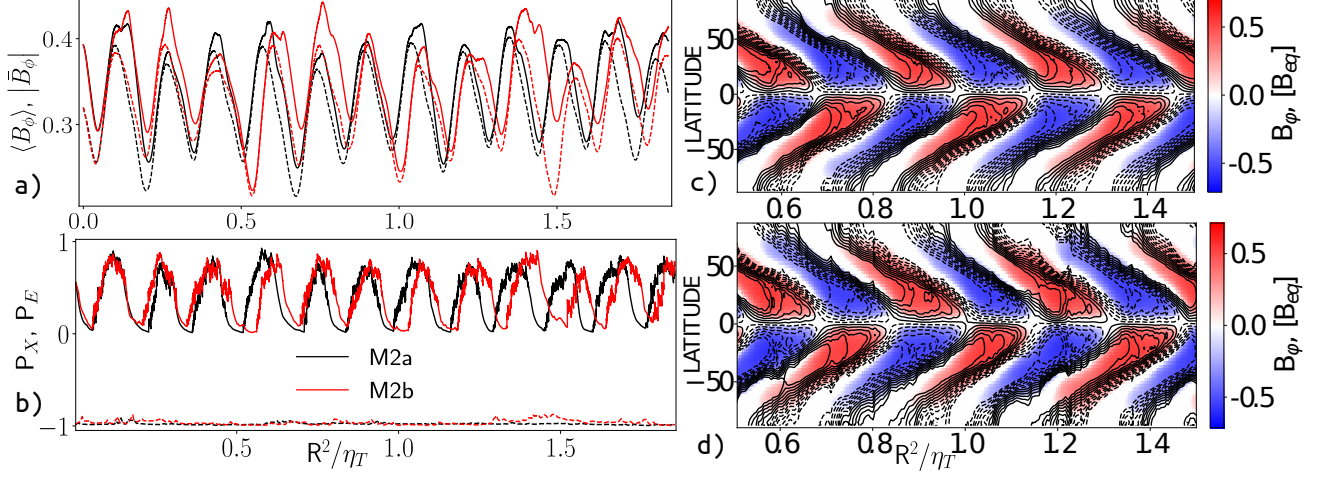


**Figure 4.** Results for models M2a (black lines) and M2b (red lines): a) the mean strength of the total toroidal magnetic field (solid lines) and the axisymmetric toroidal magnetic field (dashed lines); b) parameters  $P_X$  (solid lines) and  $P_E$  (dashed lines). The time-latitude diagram of the axisymmetric toroidal magnetic field (background image) and the radial magnetic field (contours are plotted in the range of  $\pm 0.002$ ) for: c) model M2a; d) model M2b.

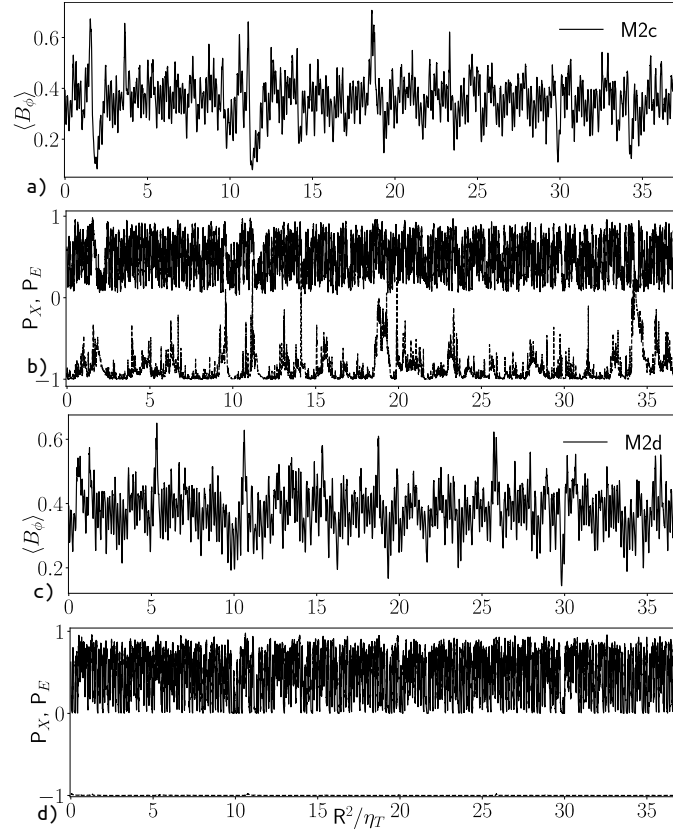


**Figure 5.** The mean strength of the total toroidal magnetic field (solid lines) for: a) model M2c and c) model M2d. Parameters  $P_X$  (solid lines) and  $P_E$  (dashed lines) for: b) model M2c and d) model M2d.

is a run without non-axisymmetric fluctuations of the  $\alpha$  effect, but with the same random realization of axisymmetric fluctuations of the  $\alpha$  effect as in model M2c. Figure 5a shows evolution of  $\langle B_\phi \rangle$  in models M2c and M2d deviate from each other shortly after beginning. Variations of parameters  $P_X$  and  $P_E$  differ substantially in models M2c and M2d.

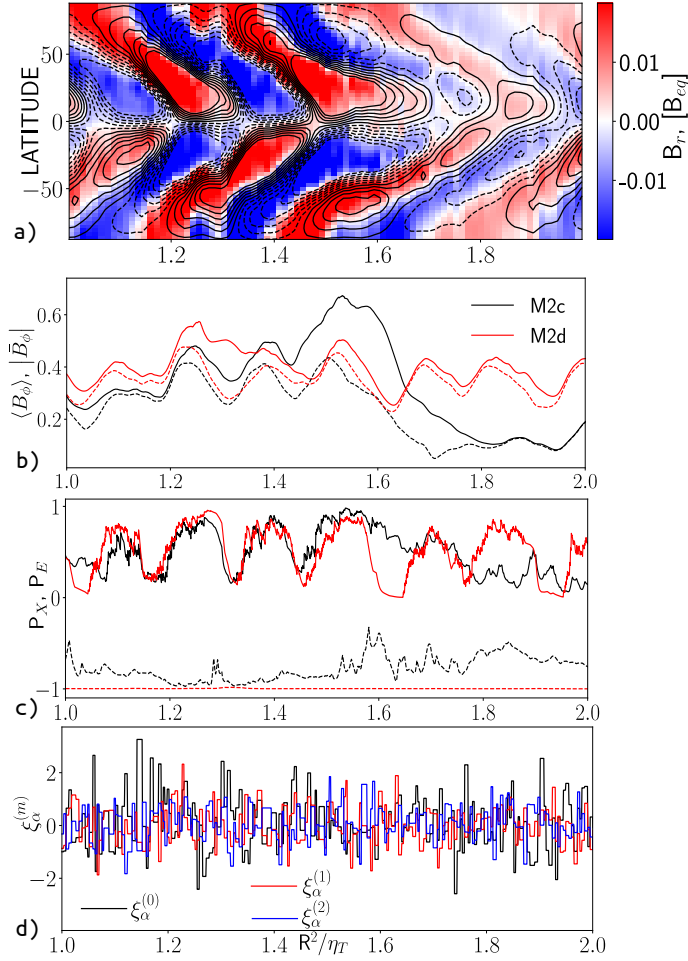


**Figure 6.** a) The time-latitude diagram of the axisymmetric toroidal magnetic field (background image) and the radial magnetic field (contours are plotted in the range of  $\pm 0.002$ ) for model M2c during the super-cycle event. b) The mean strength of the total toroidal magnetic field (solid lines) for models M2c (black) and model M2d (red) for a time interval which include the super-cycle events. c) Parameters  $P_X$  (solid lines) and  $P_E$  (dashed lines) for these models; d) random fluctuations of the axisymmetric part of the  $\alpha$  effect (black line) and the real part of the non-axisymmetric fluctuations of the modes  $m = 1$  and  $m = 2$ .

In particular,  $P_E \approx -1$  in model M2d, but in model M2c parameter  $P_E$  substantially deviates from  $-1$  indicating asymmetry of the hemispheric magnetic activity.

Another interesting feature of model M2c is the super-cycle event at the time moment,  $R^2/\eta_T \approx 1.5$  (Fig. 5a). It is illustrated in Figure 6. It is found that the super-cycle is formed by merging a strong cycle with a weak cycle that occurred during the decaying phase of the strong cycle. The super-cycle is characterized by a high level of non-axisymmetric magnetic fields activity. Also, the hemispheric asymmetry of magnetic field distributions is high during the decaying phase of the cycle.

Figures 7 and 6b,c show that the super cycle starts from quite strong ( $\langle B_r \rangle \approx 0.5 B_{eq}$ ) and also non-axisymmetric distributions of magnetic field, which is generated during the preceding minimum of magnetic activity. During the cycle maximum, superposition of the strong axisymmetric magnetic field and magnetic field of new bipolar regions produces wide magnetic ‘nests’ with the field strength:  $\langle B_r \rangle > B_{eq}$ . At the end of the super-cycle, the magnetic field remains non-axisymmetric, and is also antisymmetric relative to the equator. Simultaneously, the strength of the axisymmetric toroidal magnetic field reaches the deep minimum, see Figure 6b. Remarkably, model M2d does not show similar events. Figure 6d shows fluctuations of the axisymmetric and non-axisymmetric parts of the  $\alpha$ -effect. The period preceding the super-cycle event is characterized by a moderate level of the random fluctuations. The mean  $\alpha$ -effect changed its sign from positive to negative for a short period around time  $R^2/\eta_T \approx 1.25$ . It is unclear if this event triggered the dramatic increase of activity in the subsequent two magnetic cycles.

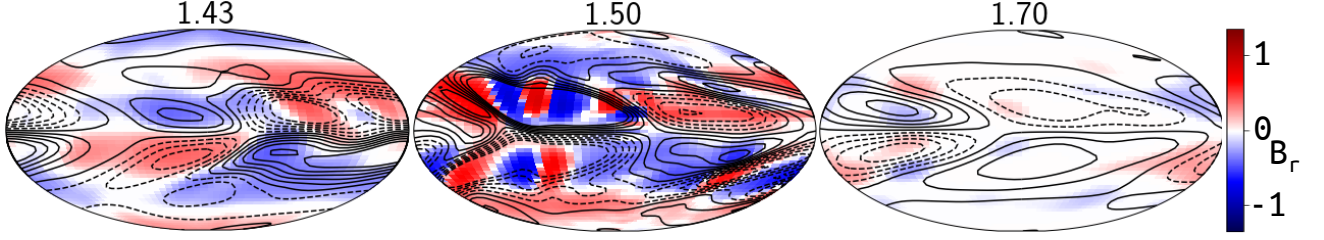


**Figure 7.** Snapshots of the radial magnetic field distribution in model M2c, contours show the  $B_\phi$  component in range of  $\pm B_{eq}$ .

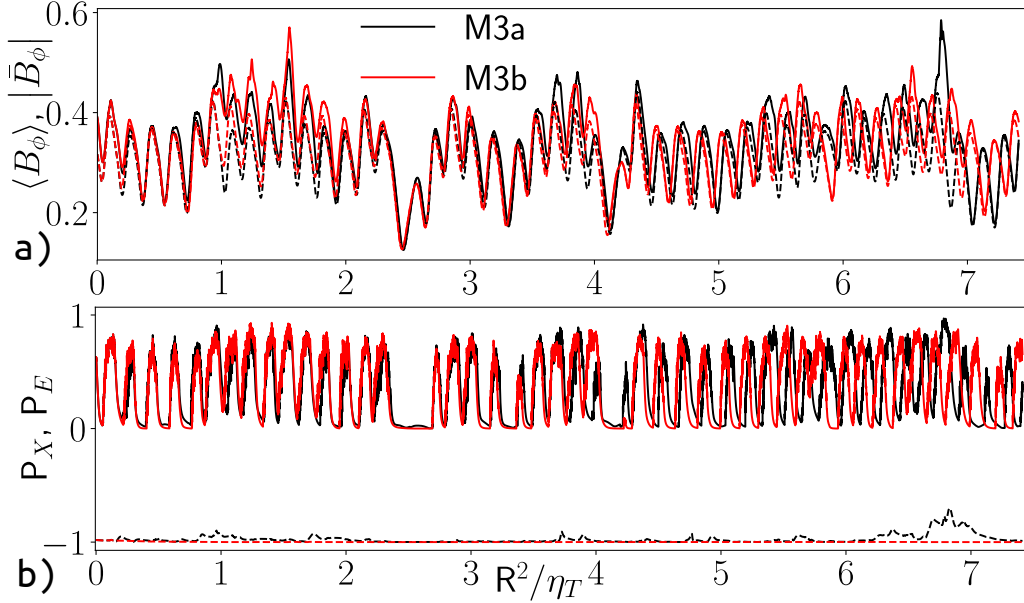


**Figure 8.** The same as Figure 4 a and b for models M3a and M3b

The case of small long-term fluctuations of  $\alpha$  is considered in models M3a and M3b, see Figure 8. These models have very similar time evolutions. The time interval in the model runs covers the period of about fifty cycles, which includes two deep minima of magnetic activity. In model M3a, there is one event which is similar to the super cycle of model M2c. Both models M3a and M3b show a high level of non-axisymmetry during the cycle maxima. In model M3b the non-axisymmetric dynamo is suppressed. This run shows strictly antisymmetric hemispheric magnetic activity. Variations of parity index  $P_E$  in model M3a are similar to those in model M2c. The higher magnitude of the non-axisymmetric variations of  $\alpha$ , the higher parity index  $P_E$ .

#### 4. COMPARISON WITH OBSERVATIONAL DATA

To compare our results with observations we use synoptic maps of radial magnetic field from the KPO, SOLIS and SDO/HMI data archives (Harvey et al. 1980; Bertello et al. 2014; Scherrer et al. 2012). Using the synoptic maps we calculate the surface mean of the unsigned radial magnetic field,  $|\langle \mathbf{B}_r \rangle|$  and the same for the axisymmetric radial magnetic field,  $|\langle \overline{\mathbf{B}}_r \rangle|$ , the parity index  $P_E$ , the level of non-axisymmetry  $P_X$ , see, Eqs (15) and (16). To calculate parameter  $P_X$  we perform the spherical harmonic decomposition up to  $m = 10$ . Results are shown in Figure 9. In agreement with the results of Stenflo (2013)  $|\langle \mathbf{B}_r \rangle|$  reaches about 20-25 G at the solar maxima. The strength of large-scale magnetic field is about a factor of two smaller than the total magnetic field strength. Figure 9b shows that  $P_X \approx 1$  during the solar maxima, and  $P_X \approx 0.5$  during the cycle minima. This means that the total basal level of the  $m = 1 \dots 11$  modes of large-scale non-axisymmetric magnetic field exceeds the basal level of the axisymmetric component of magnetic field. Parity of the axisymmetric radial magnetic field varies from  $P_E \approx 0$  during the active phase of the solar cycle to  $P_E \approx -1$  during the cycle minimum.

Figure 10 shows mean spectra of the azimuthal magnetic field distributions in our models and in the observations. Model M1a (non-axisymmetric dynamo is suppressed) shows maximum for the modes with  $m=5$  and 6. It shows

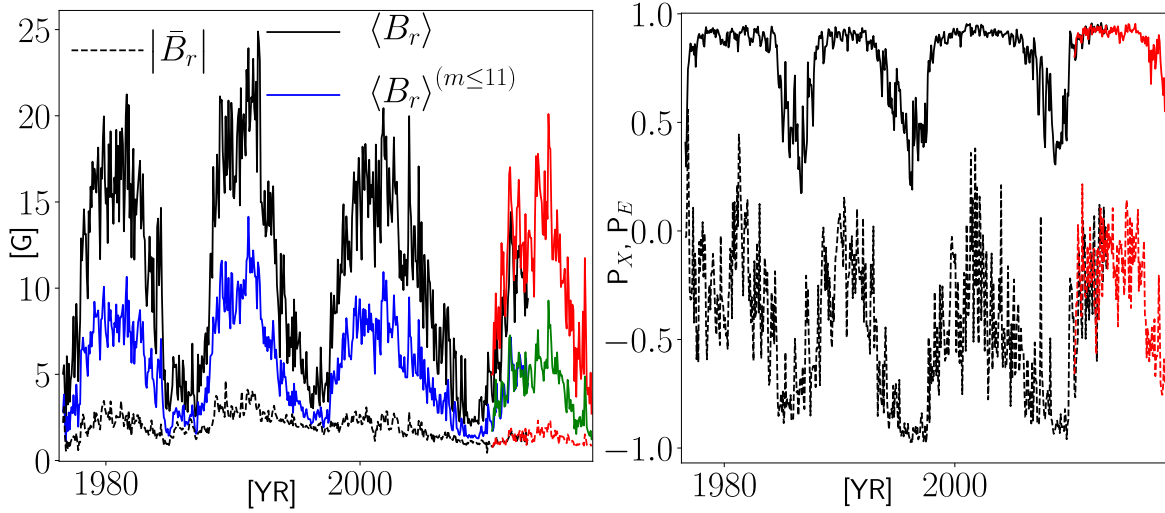


**Figure 9.** a) The unsigned radial magnetic field of the Sun from synoptic magnetograms; b) The non-axisymmetry index,  $P_X$  (solid line); The equatorial symmetry index of axisymmetric magnetic field,  $P_E$  (dashed line).

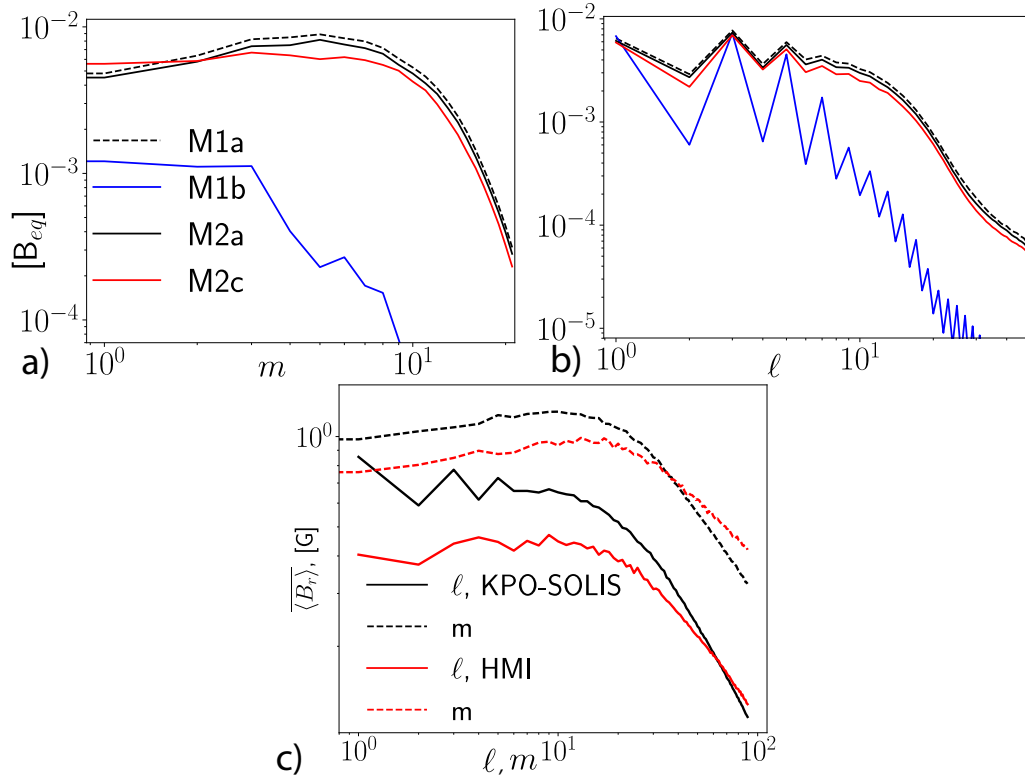


**Figure 10.** a) The mean (over latitudes and time) spectral density flux of radial magnetic field as a function of azimuthal order  $m$ ; b) the mean  $\ell$ -spectra of the radial magnetic field for the dynamo models.

a slow decrease towards small  $m$  and fast decrease for high  $m$ . The spectrum is formed by diffusive decay of the bipolar magnetic active regions. The low- $m$  branch gradually disappears with increase of the non-axisymmetric  $\alpha$ -effect perturbations. Model M1b shows a monotonic decrease of the mean magnetic field strength with the increase of  $m$ . To compare with observations we apply the FFT transform to the set of synoptic magnetograms of the radial magnetic fields. Additionally, we scale the results of our runs for  $\langle B_r \rangle$  in units of  $B_{eq}$  by a factor of 200. Figure 10 c shows comparison of the models with observations. The observational data show the maximum of the mean magnetic

field strength around  $m = 10$ . The decrease towards low  $m$  is not as strong as in model M1a, but it is similar to models M2b and M2c. We interpret this as the presence of stochastic non-axisymmetric dynamo action. In the observational data, diffusive decay of the high  $m$ -modes is less prominent than in our models. This can be interpreted in two different ways. First, the diffusion coefficient in the model may be too high. Second, the solar dynamo can be multiscale and intermittent phenomenon. These properties are not captured in our models.

Figures 10b and d show the normalized (by factor  $2\ell + 1$ )  $\ell$ -spectra of spherical harmonic decomposition of radial magnetic field for the models and observations. The observational data are processed using the Python interface of SHTools library (<https://shtools.oca.eu/shtools/index.html>). Both models and observations show a maximum for the modes of  $\ell = 3, 5$  and dips for low-degree even modes. This is in agreement with analysis of [Stenflo & Guedel \(1988\)](#); [Stenflo \(2013\)](#). As for the  $m$ -spectra, the magnetic field distribution in the models occupies a smaller spectral interval than in the real data.

## 5. DISCUSSION

We used a relatively simple 2D mean-field dynamo model to understand whether non-axisymmetric dynamo modes can be generated and maintained in the presence of random non-axisymmetric perturbations of the  $\alpha$ -effect and due to diffusive decay of emerging bipolar regions. Without such perturbations the non-axisymmetric dynamo modes do not develop, and the dynamo solutions are axisymmetric. Here, for the first time, we demonstrate that the non-axisymmetric dynamo can happen even for the solar conditions, **despite the strong differential rotation**.

The reduced 2D non-linear non-axisymmetric dynamo models considered in this paper allow us to investigate influence of the perturbations on properties of the dynamo cycles, including the degree of non-axisymmetry of the dynamo-generated magnetic field and the hemispheric asymmetry in different phases of the magnetic cycles. Despite the simplicity, the models give insight on how large-scale non-axisymmetric magnetic structures observed on the Sun may develop, as well as directions for development of more realistic non-axisymmetric dynamo models. Our model of emerging bipolar regions was based on parameterization of the Parker's buoyancy instability of the axisymmetric toroidal magnetic field. Short- and long-term stochastic large-scale (up to octupole) perturbations of the  $\alpha$ -effect of various amplitude were considered separately and in combination with the bipolar regions.

It is found that large-scale non-axisymmetric dynamo modes can be excited and maintain because of diffusion of emerging bipolar magnetic regions. Without perturbations of the  $\alpha$ -effect the non-axisymmetric magnetic field evolution affects evolution of the axisymmetric toroidal magnetic field via magnetic buoyancy. This kind of coupling was discussed previously by [Pipin & Kosovichev \(2015\)](#). In general, formation of large-scale non-axisymmetric magnetic field due to active region decay is usually accepted for granted ([Mackay & Yeates 2012](#)). Yet, the origin of the large-scale non-axisymmetric component during the solar minima is poorly understood. Our results show that remnants of decaying bipolar regions can persist during the solar minima when the cycle duration is determined by the turbulent diffusion scale.

It is found that short-term stochastic non-axisymmetric fluctuations of the  $\alpha$ -effect with the standard deviation of 25% relative to the axisymmetric level ( $\sigma_\xi = 0.25$ ) can generate weak non-axisymmetric magnetic field. Its strength is two orders of magnitude smaller than the strength of magnetic field in magnetic bipolar regions. The magnitude of turbulent  $\alpha$ -effect fluctuations is unknown. [Hoyng \(1993\)](#); [Ossendrijver & Hoyng \(1996\)](#) suggested that a high level short-term fluctuations with  $\sigma_\xi = 1$  can explain the Grand minima events. The results of [Moss et al. \(2008\)](#) showed that a low level ( $\sigma_\xi = 0.1$ ) of long-term  $\alpha$  fluctuations is another option. Our model with strong non-axisymmetric fluctuations of the  $\alpha$ -effect ( $\sigma_\xi = 1$ ) shows super-cycle events caused by a non-linear interaction of the non-axisymmetric dynamo and the process of formation of bipolar regions. The super-cycle magnitude is more than two times greater than the mean maximum of the magnetic cycles. The model run lasted 250 cycles (Fig. 5a,b) shows a few other prolonged cycles of somewhat smaller magnitudes, as well as periods of low magnetic activity, but the super-cycle events are rare.

Comparison the mean spectra of the latitudinally averaged strength of large-scale radial magnetic field with synoptic observations of solar magnetic fields during the last four cycles showed that the short-term non-axisymmetric perturbations of the  $\alpha$ -effect with  $\sigma_\xi = 0.5 - 1$  can be an option to explain the low azimuthal order part of the spectrum. Our simulations show that without the non-axisymmetric dynamo the magnetic field strength in this part of spectrum would be factor 2-3 lower than it is seen in the observational data. In comparison of our results with solar observations, we have to keep in mind that in our model the toroidal magnetic field generation and the bipolar region formation occur in the same place. Taking into account the strong effect of the differential rotation in our models and



the dominant role of the axisymmetric toroidal magnetic field, the shallow surface tachocline could be considered as a relevant place for our models. This can be different from the solar case (Brandenburg 2005). Also, our results can be applied to stars with shallow convection zones (late-F and early-G spectral classes).

Young solar analogs often show a combination of the ‘inactive’ and ‘active’ branches of the cyclic activity Oláh et al. (2009). The active branch shows long cycles (Saar & Brandenburg 1999; Böhm-Vitense 2007). Pipin & Kosovichev (2016) conjectured that the active branch can be due to the non-axisymmetric dynamo. This conclusion is supported by results of See et al. (2016). Here, for the first time we demonstrate the non-axisymmetric dynamo for a solar-type model.

VVP conducted this work as a part of FR II.16 of ISTP SB RAS. AGK thanks for support the NASA Grants NNX14AB68G, and NNX16AP05H. The dynamo code as well as codes to process the observational data are provided online by Pipin (2018)

## REFERENCES

- Berdyugina, S. V., Moss, D., Sokoloff, D., & Usoskin, I. G. 2006, *A&A*, 445, 703, doi: [10.1051/0004-6361:20053454](https://doi.org/10.1051/0004-6361:20053454)
- Bertello, L., Pevtsov, A. A., Petrie, G. J. D., & Keys, D. 2014, *SoPh*, 289, 2419, doi: [10.1007/s11207-014-0480-3](https://doi.org/10.1007/s11207-014-0480-3)
- Bigazzi, A., & Ruzmaikin, A. 2004, *ApJ*, 604, 944, doi: [10.1086/381932](https://doi.org/10.1086/381932)
- Blackman, E. G., & Brandenburg, A. 2003, *ApJL*, 584, L99, doi: [10.1086/368374](https://doi.org/10.1086/368374)
- Böhm-Vitense, E. 2007, *ApJ*, 657, 486, doi: [10.1086/510482](https://doi.org/10.1086/510482)
- Brandenburg, A. 2005, *Astrophys. J.*, 625, 539
- Brandenburg, A., Kleeorin, N., & Rogachevskii, I. 2013, *ApJ*, 776, L23, doi: [10.1088/2041-8205/776/2/L23](https://doi.org/10.1088/2041-8205/776/2/L23)
- Brandenburg, A., Krause, F., Meinel, R., Moss, D., & Tuominen, I. 1989, *A&A*, 213, 411
- Brandenburg, A., & Subramanian, K. 2005, *PhR*, 417, 1, doi: [10.1016/j.physrep.2005.06.005](https://doi.org/10.1016/j.physrep.2005.06.005)
- Cameron, R. H., & Schüssler, M. 2017, *ApJ*, 843, 111, doi: [10.3847/1538-4357/aa767a](https://doi.org/10.3847/1538-4357/aa767a)
- Choudhuri, A. R. 1992, *A&A*, 253, 277
- Getling, A. V. 2001, *Astronomy Reports*, 45, 569, doi: [10.1134/1.1383816](https://doi.org/10.1134/1.1383816)
- Glencross, W. M. 1974, *Nature*, 250, 717, doi: [10.1038/250717a0](https://doi.org/10.1038/250717a0)
- Harvey, J., Gillespie, B., Miedaner, P., & Slaughter, C. 1980, NASA STI/Recon Technical Report N, 81
- Hoyng, P. 1993, *A&A*, 272, 321
- Jennings, R., Brandenburg, A., Tuominen, I., & Moss, D. 1990, *A&A*, 230, 463
- Kitchatinov, L. L., & Pipin, V. V. 1993, *A&A*, 274, 647
- Kitiashvili, I. N., Kosovichev, A. G., Wray, A. A., & Mansour, N. N. 2010, *ApJ*, 719, 307, doi: [10.1088/0004-637X/719/1/307](https://doi.org/10.1088/0004-637X/719/1/307)
- Krause, F., & Rädler, K.-H. 1980, *Mean-Field Magnetohydrodynamics and Dynamo Theory* (Berlin: Akademie-Verlag), 271
- Kuzanyan, K. M. 1998, in *Astronomical Society of the Pacific Conference Series*, Vol. 154, *Cool Stars, Stellar Systems, and the Sun*, ed. R. A. Donahue & J. A. Bookbinder, 1286
- Leka, K. D., Barnes, G., Birch, A. C., et al. 2013, *ApJ*, 762, 130, doi: [10.1088/0004-637X/762/2/130](https://doi.org/10.1088/0004-637X/762/2/130)
- Losada, I. R., Warnecke, J., Glogowski, K., et al. 2017, in *IAU Symposium*, Vol. 327, *Fine Structure and Dynamics of the Solar Atmosphere*, ed. S. Vargas Domínguez, A. G. Kosovichev, P. Antolin, & L. Harra, 46–59
- Mackay, D. H., & Yeates, A. R. 2012, *Living Reviews in Solar Physics*, 9, 6, doi: [10.12942/lrsp-2012-6](https://doi.org/10.12942/lrsp-2012-6)
- Martin, S. F. 2018, *Frontiers in Astronomy and Space Sciences*, 5, 17, doi: [10.3389/fspas.2018.00017](https://doi.org/10.3389/fspas.2018.00017)
- Martinez Pillet, V., Moreno-Inseris, F., & Vazquez, M. 1993, *A&A*, 274, 521
- Moss, D. 1999, *MNRAS*, 306, 300, doi: [10.1046/j.1365-8711.1999.02510.x](https://doi.org/10.1046/j.1365-8711.1999.02510.x)
- Moss, D., Sokoloff, D., Usoskin, I., & Tutubalin, V. 2008, *Solar Phys.*, 250, 221
- Moss, D., Tuominen, I., & Brandenburg, A. 1990, *A&A*, 240, 142
- Noyes, R. W., Weiss, N. O., & Vaughan, A. H. 1984, *ApJ*, 287, 769, doi: [10.1086/162735](https://doi.org/10.1086/162735)
- Oláh, K., Kolláth, Z., Granzer, T., et al. 2009, *A&A*, 501, 703, doi: [10.1051/0004-6361/200811304](https://doi.org/10.1051/0004-6361/200811304)
- Ossendrijver, A. J. H., & Hoyng, P. 1996, *A&A*, 313, 959
- Parker, E. N. 1979, *Cosmical magnetic fields: Their origin and their activity* (Oxford: Clarendon Press)
- Parker, E. N. 1984, *ApJ*, 281, 839, doi: [10.1086/162163](https://doi.org/10.1086/162163)
- . 1993, *ApJ*, 408, 707, doi: [10.1086/172631](https://doi.org/10.1086/172631)
- Passos, D., Nandy, D., Hazra, S., & Lopes, I. 2014, *A&A*, 563, A18, doi: [10.1051/0004-6361/201322635](https://doi.org/10.1051/0004-6361/201322635)
- Pipin, V. 2018, *VVpipin/2DSPDy 0.1.1*, doi: [10.5281/zenodo.1413149](https://doi.org/10.5281/zenodo.1413149)



- Pipin, V. V. 2008, *Geophysical and Astrophysical Fluid Dynamics*, 102, 21
- . 2017, *MNRAS*, 466, 3007, doi: [10.1093/mnras/stw3182](https://doi.org/10.1093/mnras/stw3182)
- Pipin, V. V., & Kosovichev, A. G. 2015, *The Astrophysical Journal*, 813, 134
- Pipin, V. V., & Kosovichev, A. G. 2016, *ApJ*, 823, 133, doi: [10.3847/0004-637X/823/2/133](https://doi.org/10.3847/0004-637X/823/2/133)
- Pipin, V. V., Moss, D., Sokoloff, D., & Hoeksema, J. T. 2014, *A&A*, 567, A90, doi: [10.1051/0004-6361/201323319](https://doi.org/10.1051/0004-6361/201323319)
- Pipin, V. V., & Sokoloff, D. D. 2011, *Physica Scripta*, 84, 065903
- Pipin, V. V., Sokoloff, D. D., & Usoskin, I. G. 2012, *A&A*, 542, A26, doi: [10.1051/0004-6361/201118733](https://doi.org/10.1051/0004-6361/201118733)
- Raedler, K.-H. 1986, *Astronomische Nachrichten*, 307, 89, doi: [10.1002/asna.2113070205](https://doi.org/10.1002/asna.2113070205)
- Raedler, K.-H., Wiedemann, E., Brandenburg, A., Meinel, R., & Tuominen, I. 1990, *A&A*, 239, 413
- Rüdiger, G., Kitchatinov, L. L., & Brandenburg, A. 2011, *SoPh*, 269, 3, doi: [10.1007/s11207-010-9683-4](https://doi.org/10.1007/s11207-010-9683-4)
- Saar, S. H., & Brandenburg, A. 1999, *ApJ*, 524, 295, doi: [10.1086/307794](https://doi.org/10.1086/307794)
- Scherrer, P. H., Schou, J., Bush, R. I., et al. 2012, *SoPh*, 275, 207, doi: [10.1007/s11207-011-9834-2](https://doi.org/10.1007/s11207-011-9834-2)
- See, V., Jardine, M., Vidotto, A. A., et al. 2016, *MNRAS*, 462, 4442, doi: [10.1093/mnras/stw2010](https://doi.org/10.1093/mnras/stw2010)
- Stein, R. F., & Nordlund, Å. 2012, *ApJL*, 753, L13, doi: [10.1088/2041-8205/753/1/L13](https://doi.org/10.1088/2041-8205/753/1/L13)
- Stenflo, J. O. 2012, *A&A*, 547, A93, doi: [10.1051/0004-6361/201219833](https://doi.org/10.1051/0004-6361/201219833)
- . 2013, *A&A Rv*, 21, 66, doi: [10.1007/s00159-013-0066-3](https://doi.org/10.1007/s00159-013-0066-3)
- Stenflo, J. O., & Guedel, M. 1988, *A&A*, 191, 137
- Stix, M. 1977, *A&A*, 59, 73
- Usoskin, I. G., Sokoloff, D., & Moss, D. 2009, *SoPh*, 254, 345, doi: [10.1007/s11207-008-9293-6](https://doi.org/10.1007/s11207-008-9293-6)
- Wang, Y.-M., & Sheeley, Jr., N. R. 1990, *ApJ*, 355, 726, doi: [10.1086/168805](https://doi.org/10.1086/168805)